Magazine of Civil Engineering

ISSN 2712-8172

journal homepage: http://engstroy.spbstu.ru/

Research article

UDC 69.04

DOI: 10.34910/MCE.126.3

Validating the predicted axial strength of FRP-reinforced concrete circular columns

M.Q. Kadhim ✉, ***H.F. Hassan***

College of Engineering, Mustansiriyah University, Baghdad, Iraq

✉ *mohamedq1992@uomustansiriyah.edu.iq*

Keywords: fiber reinforced polymers, axial load, circular columns, spirals, hoops, experimental load

Abstract. Over the last three decades, researchers have significantly contributed to advancing fiber-reinforced polymer (FRP) bars to address corrosion issues in conventional steel reinforcement bars embedded in components of reinforced concrete structures. This research aimed to establish an ideal allowable axial compression load for concrete columns reinforced with FRP using data from previous studies. This article compares and explains the contrasts of several of the most popular FRP codes (ACI, CSA, and JSCE) with one equation proposed in previous research using empirical information gleaned from the literature review. The models' statistical analysis compares theoretical and practical loads, Young's modulus, concrete strength, longitudinal reinforcement ratio, and transverse reinforcement ratio for hoops and spirals. Estimating the effect of FRP longitudinal bars on the applied load carried by FRP-reinforced concrete columns can be done with the help of an empirical equation that uses the compressive strength of concrete to estimate the axial stress of FRP longitudinal bars in concrete columns. Results from the CSA and the ACI were almost similar, and both were superior to those from the JSCE in terms of being ideal, consistent, and safe. The results for modulus of elasticity, concrete compressive strength, and transverse reinforcement ratio for spiral reinforcement were more stable, according to the CSA. In contrast, according to the ACI, results for longitudinal and transverse reinforcement ratios of hoop reinforcement were more stable and secure. Lastly, the previously proposed equation is the best way to determine the transverse reinforcement ratio for hoop reinforcement and the compressive strength of concrete from all codes. In conclusion, the previously proposed equation is the most effective for calculating the transverse reinforcement ratio for hoop reinforcement and compressive strength.

Citation: Kadhim, M.Q., Hassan, H.F. Validating the predicted axial strength of FRP-reinforced concrete circular columns. Magazine of Civil Engineering. 2024. 17(2). Article no. 10.34910/MCE.126.3. DOI: 10.34910/MCE.126.3

1. Introduction

The primary function of a reinforced concrete column is to sustain axial loads with or without bending moments. Due to the corrosion of steel bars, the axial load-carrying capacity of steel bar-reinforced concrete columns decreases over the concrete structures' service life, especially in coastal regions or harsh environments. The cost of rehabilitating and repairing deteriorated concrete structures is significantly high [1]. The literature review found that FRP composites can be used in various civil/structural applications. The FRP composites have various structural forms that can be classified into two main classes: 1) external reinforcement (FRP jacketing) and 2) internal reinforcement (FRP reinforcing bars). There are four common varieties of FRP: aramid (AFRP), basalt (BFRP), glass (GFRP), and carbon (CFRP) fibers, all encased in the polymer [2, 3]. FRP composites, including FRP bars, possess many advantageous characteristics, such as resistance to harsh environmental conditions, lightweight, and high tensile strength [4, 5]. Hence, FRP bars have the potential to replace steel bars and overcome the deterioration of concrete structures associated with the corrosion of steel reinforcement. However, using FRP bars as reinforcement in

compression members is still not recommended. This is because the FRP bar's ultimate compressive strength is considerably lower than its ultimate tensile strength [6]. De Luca et al. [7] investigated five square concrete columns subjected to axial load. They concluded that GFRP bars could be used in columns, but their contribution could be ignored when calculating nominal capacity. Moreover, they found that GFRP hoops did not grow longitudinal bars' ultimate capacity but reduced their bend. Kobayashi and Fujisaki [8] conducted experiments with bars made of AFRP, CFRP, and GFRP. The compressive strengths of CFRP, AFRP, and GFRP reinforcement bars were 30–50 %, 10 %, and 30–40 % of their tensile strength, respectively. Deitz et al. [9] conducted compression tests on 45 GFRP bars (15-mm diameter with unbraced lengths varying from 50 to 380 mm). Based on the experiments' outcomes, the average ultimate compressive strength was nearly 50% of the average ultimate tensile strength. However, the compression modulus was about the same as that of tension. Alsayed et al. [10] tested fifteen 450×250×1200 mm concrete columns under concentric axial loads to determine the effect of replacing longitudinal and transverse steel reinforcing bars with an equivalent amount of GFRP reinforcement. GFRP reinforcing bars reduced column axial capacity by 13 %. GFRP hoops reduced axial capacity by 10%, regardless of the longitudinal bar type. Up to 80% of the column's ultimate capacity, replacing steel hoops with GFRP hoops did not affect load deformation. Tobbi et al. [11] and Afifi et al. [12] reported that GFRP and CFRP longitudinal bars can contribute up to 10% and 13%, respectively, to the axial load-carrying capacity of the concrete columns. Hadhood et al. [13] conducted an experimental investigation on the concentric and eccentric behavior of full-scale circular high-strength concrete (HSC) columns reinforced with GFRP bars and spirals. A total of 10 columns were tested under monotonic loading with different eccentricities. The test variables were the eccentricity-to-diameter ratio and the longitudinal-reinforcement ratio. Compression failure in the concrete controlled the ultimate capacity of specimens tested under small eccentric loads. However, a flexural-tension failure initiated in specimens tested under high eccentric loading resulted from excessive axial and lateral deformations and cracks on the tension side until a secondary compression and stability failure occurred due to the concrete's strain limitations. Longitudinal GFRP bars contributed about 5% of the axial load capacity of GFRP-HSC columns. Hadi et al. [14] conducted a study on the use of GFRP bars in HSC. It was observed that the GFRP bar-reinforced HSC specimens sustained a similar axial load under concentric axial compression compared to their steel counterparts, but the efficiency of GFRP bar-reinforced HSC specimens in sustaining axial loads decreased with an increase in the axial load eccentricity. Direct replacement of steel reinforcement with the same amount of GFRP reinforcement in HSC specimens resulted in about 30% less ductility under a concentric axial load. In CAN/CSA S806-12 [15] or ACI 440.1R-15 [16], no theoretical equation was proposed to predict the maximum axial load capacity of FRP bar-reinforced concrete columns. This is because of the variances in the reported ultimate compressive strength of the FRP bars and their contribution as longitudinal reinforcement in concrete columns. However, previous research gave many theoretical equations for predicting the maximum axial loads that FRP bar-reinforced concrete columns could carry. The issue of utilizing FRP as a substitute for traditional reinforcing steel in compression members has yet to be evaluated through available equations and whether these equations can be used for design purposes. As we mentioned, there are available equations, but they have yet to be evaluated through many models. Thus, in this research, we will evaluate the most prominent four equations to determine the validity of their use for design purposes based on a wide range of experimental data collected from previous studies. This statistical analysis predicted the maximum axial load capacity of concrete columns reinforced longitudinally with FRP bars and studied other factors based on many codes and one significant suggested equation from earlier studies.

Table 1. Experimental data of FRP bar reinforced concrete columns taken from available previous research studies.

No.	The specimen reference	Specimen cross-section			FRP longitudinal reinforcement				FRP transverse reinforcement		$f'c$
		Specimen	Column shape	Diameters (mm)	Type	ρ_{fl} (%)	f_{fu} (MPa)	E_f (MPa)	Type	ρ_{ft} (%)	(MPa)
1	Pantelides et al. [17]	#13GLCTL	Circular	254	GFRP bars	1.60	740	43300	GFRP spirals	1.70	36
2		#14GLCTL	Circular	254	GFRP bars	1.60	740	43300	GFRP spirals	1.70	36
3	Afifi et al. [12]	C6V-3H80	Circular	300	CFRP bars	1.00	1899	140000	CFRP spirals	1.50	42.90
4		C10V-3H80	Circular	300	CFRP bars	1.70	1899	140000	CFRP spirals	1.50	42.90
5		C14V-3H80	Circular	300	CFRP bars	2.40	1899	140000	CFRP spirals	1.50	42.90
6		C10V-2H80	Circular	300	CFRP bars	1.70	1899	140000	CFRP spirals	0.70	42.90
7		C10V-4H80	Circular	300	CFRP bars	1.70	1899	140000	CFRP spirals	2.70	42.90

No.	The specimen reference	Specimen cross-section			FRP longitudinal reinforcement				FRP transverse reinforcement		$f'c$ (MPa)
		Specimen	Column shape	Diameters (mm)	Type	ρ_{fl} (%)	f_{fu} (MPa)	E_f (MPa)	Type	ρ_{ft} (%)	
8	Afifi et al. [18]	C10V-3H40	Circular	300	CFRP bars	1.70	1899	140000	CFRP spirals	3.00	42.90
9		C10V-3H120	Circular	300	CFRP bars	1.70	1899	140000	CFRP spirals	1.00	42.90
10		C10V-2H35	Circular	300	CFRP bars	1.70	1899	140000	CFRP spirals	1.50	42.90
11		C10V-4H145	Circular	300	CFRP bars	1.70	1899	140000	CFRP spirals	1.50	42.90
12		G8V-3H80	Circular	300	GFRP bars	2.20	934	55400	GFRP spirals	1.50	42.90
13		G4V-3H80	Circular	300	GFRP bars	1.10	934	55400	GFRP spirals	1.50	42.90
14		G12V-3H80	Circular	300	GFRP bars	3.20	934	55400	GFRP spirals	1.50	42.90
15		G8V-2H80	Circular	300	GFRP bars	2.20	934	55400	GFRP spirals	**0.70**	42.90
16		G8V-4H80	Circular	300	GFRP bars	2.20	934	55400	GFRP spirals	2.70	42.90
17		G8V-3H40	Circular	300	GFRP bars	2.20	934	55400	GFRP spirals	3.00	42.90
18		G8V-3H120	Circular	300	GFRP bars	2.20	934	55400	GFRP spirals	1.00	42.90
19		G8V-2H35	Circular	300	GFRP bars	2.20	934	55400	GFRP spirals	1.50	42.90
20		G8V-4H145	Circular	300	GFRP bars	2.20	934	55400	GFRP spirals	1.50	42.90
21	Mohamed et al. [19]	G2S	Circular	300	GFRP bars	2.24	934	55400	GFRP spirals	0.70	42.90
22		G3S	Circular	300	GFRP bars	2.24	934	55400	GFRP spirals	1.50	42.90
23		G4S	Circular	300	GFRP bars	2.24	934	55400	GFRP spirals	2.70	42.90
24		G3H200	Circular	300	GFRP bars	2.24	934	55400	GFRP hoops	1.50	42.90
25		G3H400	Circular	300	GFRP bars	2.24	934	55400	GFRP hoops	1.50	42.90
26		G3H600	Circular	300	GFRP bars	2.24	934	55400	GFRP hoops	1.50	42.90
27		C2S	Circular	300	CFRP bars	1.79	1899	140000	CFRP spirals	0.70	42.90
28		C3S	Circular	300	CFRP bars	1.79	1899	140000	CFRP spirals	1.50	42.90
29		C4S	Circular	300	CFRP bars	1.79	1899	140000	CFRP spirals	2.70	42.90
30		C3H200	Circular	300	CFRP bars	1.79	1899	140000	CFRP hoops	1.50	42.90
31		C3H400	Circular	300	CFRP bars	1.79	1899	140000	CFRP hoops	1.50	42.90
32		C3H600	Circular	300	CFRP bars	1.79	1899	140000	CFRP hoops	1.50	42.90
33	Karim et al. [20]	G6-G60	Circular	205	GFRP bars	2.30	1600	66000	GFRP spirals	2.97	37
34		G6-G30	Circular	205	GFRP bars	2.30	1600	66000	GFRP spirals	5.94	37
35		00-G60	Circular	205	-	0.00	0.00	0.00	GFRP spirals	2.97	37
36		00-G30	Circular	205	-	0.00	0.00	0.00	GFRP spirals	5.94	37
37	Maranan et al. [21]	C-8-00	Circular	250	GFRP bars	2.43	1184	62600	-	-	38
38		GGC-8-H50	Circular	250	GFRP bars	2.43	1184	62600	GFRP hoops	3.13	38
39		GGC-8-H100	Circular	250	GFRP bars	2.43	1184	62600	GFRP hoops	1.57	38
40		GGC-8-H200	Circular	250	GFRP bars	2.43	1184	62600	GFRP hoops	0.78	38
41		GGC-8-S50	Circular	250	GFRP bars	2.43	1184	62600	GFRP spirals	3.13	38

No.	The specimen reference	Specimen cross-section			FRP longitudinal reinforcement				FRP transverse reinforcement		$f'c$ (MPa)
		Specimen	Column shape	Diameters (mm)	Type	ρ_{fl} (%)	f_{fu} (MPa)	E_f (MPa)	Type	ρ_{ft} (%)	
42		GGC-8-S100	Circular	250	GFRP bars	2.43	1184	62600	GFRP spirals	1.57	38
43		GGC-16-H100	Circular	250	GFRP bars	2.43	1184	62600	GFRP hoops	1.57	38
44		GGC-16-S100	Circular	250	GFRP bars	2.43	1184	62600	GFRP spirals	1.57	38
45	Hadi et al. [14]	G60E0	Circular	210	GFRP bars	2.19	1190	52000	GFRP spirals	2.94	85
46		G30E0	Circular	210	GFRP bars	2.19	1190	52000	GFRP spirals	5.88	85
47	Hadhood et al. [22]	C1-I	Circular	305	GFRP bars	2.18	1289	54900	GFRP spirals	1.44	35
48		C1-II	Circular	305	GFRP bars	3.27	1289	54900	GFRP spirals	1.44	35
49	Abdelazim et al. [23]	C1	Circular	305	GFRP bars	2.19	1449	61800	GFRP spirals	1.17	46.60
50		C2	Circular	305	GFRP bars	2.19	1449	61800	GFRP spirals	1.17	46.60
51		C3	Circular	305	GFRP bars	2.19	1449	61800	GFRP spirals	1.17	46.60
52		C4	Circular	305	GFRP bars	2.19	1449	61800	GFRP spirals	1.17	46.60
53		C5	Circular	305	GFRP bars	2.19	1449	61800	GFRP spirals	1.17	46.60
54	Raza et al. [24]	GH75-C	Circular	250	GFRP bars	1.57	794	50000	GFRP hoops	1.42	37.66
55		GH150-C	Circular	250	GFRP bars	1.57	794	50000	GFRP hoops	0.71	37.66
56		GS38-C	Circular	250	GFRP bars	1.57	794	50000	GFRP spirals	2.84	37.66
57		GS75-C	Circular	250	GFRP bars	1.57	794	50000	GFRP spirals	1.42	37.66
58	El-Gamal and Alshareedah [25]	G1 (6G12-G75)	Circular	230	GFRP bars	1.63	1113	62300	GFRP spirals	2.20	25.40
59		G6 (6G12-G75)	Circular	230	GFRP bars	1.63	1250	61400	GFRP spirals	2.20	25.40
60		G2 (8G12-G75)	Circular	230	GFRP bars	2.17	1113	62300	GFRP spirals	2.20	25.40
61		G3 (8G16-G75)	Circular	230	GFRP bars	3.87	1102	61200	GFRP spirals	2.20	25.40
62		G4 (6G12-G100)	Circular	230	GFRP bars	1.63	1113	62300	GFRP spirals	1.65	25.40
63		G5 (6G12-G50)	Circular	230	GFRP bars	1.63	1113	62300	GFRP spirals	3.30	25.40
64	Elchalakani et al. [26]	G3-120-C	Circular	215	GFRP bars	0.55	930	59000	GFRP spirals	0.94	34
65		G4-120-C	Circular	215	GFRP bars	0.73	930	59000	GFRP spirals	0.94	34
66		G5-120-C	Circular	215	GFRP bars	0.92	930	59000	GFRP spirals	0.94	34
67		G4-40-C	Circular	215	GFRP bars	0.73	930	59000	GFRP spirals	2.75	34
68		G4-80-C	Circular	215	GFRP bars	0.73	930	59000	GFRP spirals	1.39	34
69	Elhamaymy et al. [27]	GCP-80S	Circular	304	GFRP bars	2.18	1389	52500	GFRP spirals	1.50	40
70		GCP-80S-22	Circular	304	GFRP bars	2.18	1389	52500	GFRP spirals	1.50	40
71		GCP-80S-60	Circular	304	GFRP bars	2.18	1389	52500	GFRP spirals	1.50	40
72		GCP-40S	Circular	304	GFRP bars	2.18	1389	52500	GFRP spirals	3.00	40
73		GCP-40S-22	Circular	304	GFRP bars	2.18	1389	52500	GFRP spirals	3.00	40
74		GCP-40S-60	Circular	304	GFRP bars	2.18	1389	52500	GFRP spirals	3.00	40
75		GCP-120S	Circular	304	GFRP bars	2.18	1389	52500	GFRP spirals	1.00	40

No.	The specimen reference	Specimen cross-section			FRP longitudinal reinforcement				FRP transverse reinforcement		$f'c$ (MPa)
		Specimen	Column shape	Diameters (mm)	Type	ρ_{fl} (%)	f_{fu} (MPa)	E_f (MPa)	Type	ρ_{ft} (%)	
76		GCP-120S-22	Circular	304	GFRP bars	2.18	1389	52500	GFRP spirals	1.00	40
77		GCP-120S-60	Circular	304	GFRP bars	2.18	1389	52500	GFRP spirals	1.00	40
78		GCP-80-O	Circular	304	GFRP bars	2.18	1389	52500	GFRP hoops	1.50	40
79		GCP-80-O-22	Circular	304	GFRP bars	2.18	1389	52500	GFRP hoops	1.50	40
80		GCP-80-O-60	Circular	304	GFRP bars	2.18	1389	52500	GFRP hoops	1.50	40
81	Bakouregui et al. [28]	G-8-0	Circular	305	GFRP bars	2.20	1289	54900	GFRP spirals	1.44	52
82		B-8-0	Circular	305	BFRP bars	2.20	1724	64800	GFRP spirals	1.44	52
83	Gouda et al. [29]	SC-6G-80	Circular	305	GFRP bars	1.63	1289	54900	GFRP spirals	0.95	34.70
84		SC-8G-80	Circular	305	GFRP bars	2.18	1289	54900	GFRP spirals	0.95	34.70
85		SC-12G-80	Circular	305	GFRP bars	3.27	1289	54900	GFRP spirals	0.95	34.70
86	Tang et al. [30]	fh-f-2	Circular	150	BFRP bars	5.50	1100	50000	BFRP spirals	7.30	65
87		fh-f-4	Circular	150	BFRP bars	5.50	1100	50000	BFRP spirals	3.70	53
88		fh-f-8	Circular	150	BFRP bars	5.50	1100	50000	BFRP spirals	1.80	42
89		fl-f-2	Circular	150	BFRP bars	3.10	1250	50000	BFRP spirals	7.30	55
90		fl-f-4	Circular	150	BFRP bars	3.10	1250	50000	BFRP spirals	3.70	43
91		fl-f-8	Circular	150	BFRP bars	3.10	1250	50000	BFRP spirals	1.80	35

f_{fu} is the ultimate tensile strength of FRP bars.

E_f is the modulus of elasticity of FRP bars.

$f'c$ is the compressive strength of the concrete.

2. Methods

A collection of 91 FRP RC columns that failed under axial compression was made to study their behavior in axial compression and evaluate the design codes and previously proposed equation [12, 14, 17–30]. Specimens had long and short columns. Data from many studies were clearly reported. However, other calculations used individual parameters to determine parameter values separately. The column results were unaffected. The compression design parameters are summarized in Table 2. The column diameter D was 150–305 mm. Diameter cores D_c range from 104 to 237.2 mm. Column lengths L varied from 300 mm to 2,500 mm. During the test day, the concrete cylinder strength, f_c', was between 25.4 and 85 MPa. The gross area, A_g was found to be in the range from 17671.46 to 73061.66 mm^2 where it was reported. The longitudinal reinforcement ratio $\left(\rho_{ft} = n \times A_b / A_g\right)$, where n is the number of longitudinal reinforcements, A_b is the area of the FRP bar, and A_g is the gross sectional area, was between 0.00 and 5.5 %. The transverse reinforcement ratio $\left(\rho_{ft} = 4 \times A_{ft} / D_c \times s\right)$, where A_{ft} is the area of the FRP bar of transverse reinforcement, D_c is the diameter of the core, and s is the spacing between hoops of reinforcement or the pitch of the spiral reinforcement) ranged from 0.00 to 7.3 %. The longitudinal reinforcement's elasticity modulus, E_{ft}, varied from 0 to 140 GPa. The transverse reinforcement's elasticity modulus, E_{ft}, varied from 0 to 140 GPa. The longitudinal reinforcement's tensile strength, f_{ful},

wide-ranging 0 toward 1,899 MPa. Also, the transverse reinforcement's tensile strength is a wide range, f_{ful}, varied from 0 toward 1,899 MPa.

Table 2. Compression design parameters for columns used in the database.

Number of columns	Database				
	91				
Properties	Min	Max	SD	Avg	COV (%)
D (mm)	150.00	305.00	46.65	268.25	17.39
D_c (mm)	104.00	237.20	40.21	203.69	19.74
A_g (mm^2)	17671.46	73061.66	17790.53	58207.06	30.56
R(mm)	75.00	152.50	23.32	134.13	17.39
L(mm)	300.00	2500.00	403.79	1245.85	32.41
L/R	4.00	16.39	2.55	9.16	27.86
ρ_{ft} (%)	0.00	5.50	0.89	2.12	41.85
f_{ful} (MPa)	0.00	1899.00	393.26	1253.60	31.37
E_{ft} (MPa)	0.00	140000.00	33215.50	68729.67	48.33
ρ_{ft} (%)	0.00	7.30	1.34	1.98	67.76
f_{ful} (MPa)	0.00	1899.00	336.65	1227.52	27.42
E_{ft} (MPa)	0.00	140000.00	27859.66	66413.19	41.95
f'_c (MPa)	25.40	85.00	9.11	41.08	22.18

Table 3. Comparison between the experimental and theoretical axial load-carrying capacity of FRP bar-reinforced concrete columns available in the previous research studies.

No.	The study	Specimen	$P_{exp.}$ [a]	$P_o / P_{exp.}$ [b]			
				Eq. (5)	Eq. (5)	Eq. (2.1 or 2.2)	Eq. (3)
				ACI 318-19 [31] c	CSA A23.3-19 [32] c	JSCE 1997 [33]	Tobbi et al. [11] d
1	Pantelides et al. [17]	#13GLCTL	1975	0.83	0.83	0.60	0.88
2		#14GLCTL	1788	0.91	0.92	0.67	0.97
3	Afifi et al. [12]	C6V-3H80	2905	0.99	1.01	0.68	1.05
4		C10V-3H80	3013	1.02	1.05	0.66	1.12
5		C14V-3H80	3107	1.05	1.09	0.64	1.19
6		C10V-2H80	2948	1.04	1.07	0.67	1.14
7		C10V-4H80	3147	0.97	1.00	0.63	1.07
8		C10V-3H40	3070	1.00	1.03	0.65	1.10
9		C10V-3H120	2981	1.03	1.06	0.67	1.13
10		C10V-2H35	3148	0.97	1.00	0.63	1.07
11		C10V-4H145	2941	1.04	1.07	0.67	1.15
12	Afifi et al. [18]	G8V-3H80	2920	0.95	0.97	0.68	1.04
13		G4V-3H80	2826	0.95	0.96	0.70	0.99
14		G12V-3H80	2998	0.96	0.98	0.66	1.09
15		G8V-2H80	2857	0.97	0.99	0.69	1.06
16		G8V-4H80	3019	0.92	0.94	0.66	1.01
17		G8V-3H40	2964	0.94	0.95	0.67	1.03
18		G8V-3H120	2804	0.99	1.01	0.71	1.08
19		G8V-2H35	2951	0.94	0.96	0.67	1.03
20		G8V-4H145	2865	0.97	0.99	0.69	1.06
21		G2S	2857	0.97	0.99	0.69	1.06

No.	The study	Specimen	$P_{exp.}$ [a]	$P_o / P_{exp.}$ [b]			
				Eq. (5)	Eq. (5)	Eq. (2.1 or 2.2)	Eq. (3)
				ACI 318-19 [31] c	CSA A23.3-19 [32] c	JSCE 1997 [33]	Tobbi et al. [11] d
22	Mohamed et al. [19]	G3S	2920	0.95	0.97	0.68	1.04
23		G4S	3019	0.92	0.94	0.66	1.01
24		G3H200	2840	0.98	1.00	0.70	1.07
25		G3H400	2871	0.97	0.98	0.69	1.06
26		G3H600	2935	0.95	0.96	0.68	1.04
27		C2S	2948	1.04	1.07	0.67	1.14
28		C3S	3013	1.02	1.05	0.66	1.12
29		C4S	3147	0.97	1.00	0.63	1.07
30		C3H200	2869	1.07	1.10	0.69	1.18
31		C3H400	2960	1.03	1.06	0.67	1.14
32		C3H600	3008	1.02	1.05	0.66	1.12
33	Karim et al. [20]	G6-G60	1425	0.82	0.83	0.56	1.01
34		G6-G30	2041	0.57	0.58	0.39	0.71
35		00-G60	940	1.10	1.10	0.85	1.10
36		00-G30	1343	0.77	0.77	0.59	0.77
37	Maranan et al. [21]	GGC-8-00	1772	1.00	1.02	0.69	1.15
38		GGC-8-H50	1791	0.99	1.01	0.68	1.14
39		GGC-8-H100	1981	0.89	0.91	0.62	1.03
40		GGC-8-H200	1988	0.89	0.91	0.61	1.03
41		GGC-8-S50	1838	0.96	0.98	0.66	1.11
42		GGC-8-S100	2063	0.86	0.88	0.59	0.99
43		GGC-16-H100	1624	1.09	1.11	0.75	1.26
44		GGC-16-S100	1208	1.47	1.50	1.01	1.69
45	Hadi et al. [14]	G60E0	2721	0.95	0.96	0.71	1.05
46		G30E0	2593	1.00	1.01	0.74	1.10
47	Hadhood et al. [22]	C1-I	2608	0.92	0.93	0.64	1.09
48		C1-II	2670	0.93	0.96	0.63	1.19
49	Abdelazim et al. [23]	C1	3535	0.88	0.90	0.63	1.03
50		C2	3490	0.90	0.91	0.64	1.04
51		C3	3453	0.91	0.92	0.64	1.05
52		C4	3359	0.93	0.95	0.66	1.08
53		C5	3331	0.94	0.95	0.67	1.09
54	Raza et al. [24]	GH75-C	2290.51	0.73	0.73	0.53	0.77
55		GH150-C	1965.8	0.84	0.85	0.61	0.89
56		GS38-C	2678.1	0.62	0.63	0.45	0.66
57		GS75-C	2403.54	0.69	0.70	0.50	0.73
58	El-Gamal and AlShareedah [25]	G1 (6G12-G75)	1202	0.84	0.86	0.57	0.95
59		G6 (6G12-G75)	1166	0.86	0.88	0.59	1.01
60		G2 (8G12-G75)	1536	0.68	0.70	0.45	0.80
61		G3 (8G16-G75)	1457	0.79	0.83	0.47	1.02
62		G4 (6G12-G100)	1065	0.95	0.97	0.65	1.08
63		G5 (6G12-G50)	1585	0.64	0.65	0.44	0.72
64	Elchalakani et al. [26]	G3-120-C	943	1.15	1.16	0.86	1.19
65		G4-120-C	1031	1.06	1.07	0.78	1.11
66		G5-120-C	1286	0.86	0.87	0.63	0.91
67		G4-40-C	1223	0.90	0.90	0.66	0.93
68		G4-80-C	1088	1.01	1.02	0.74	1.05
69	Elhamaymy et al. [27]	GCP-80S	2850	0.93	0.95	0.67	1.12
70		GCP-80S-22	3200	0.83	0.85	0.59	1.00
71		GCP-80S-60	3350	0.80	0.81	0.57	0.95
72		GCP-40S	2900	0.92	0.93	0.65	1.10

No.	The study	Specimen	$P_{exp.}$ [a]	$P_o / P_{exp.}$ [b]			
				Eq. (5)	Eq. (5)	Eq. (2.1 or 2.2)	Eq. (3)
				ACI 318-19 [31] c	CSA A23.3-19 [32] c	JSCE 1997 [33]	Tobbi et al. [11] d
73		GCP-40S-22	3100	0.86	0.87	0.61	1.03
74		GCP-40S-60	3450	0.77	0.78	0.55	0.92
75		GCP-120S	2800	0.95	0.97	0.68	1.14
76		GCP-120S-22	3000	0.89	0.90	0.63	1.06
77		GCP-120S-60	3250	0.82	0.83	0.58	0.98
78		GCP-80-O	2700	0.99	1.00	0.70	1.18
79		GCP-80-O-22	3100	0.86	0.87	0.61	1.03
80		GCP-80-O-60	3300	0.81	0.82	0.58	0.97
81	Bakouregui et al. [28]	G-8-0	3530	0.97	0.98	0.70	1.10
82		B-8-0	3530	0.98	1.00	0.70	1.17
83	Gouda et al. [29]	SC-6G-80	2550	0.91	0.92	0.65	1.04
84		SC-8G-80	2700	0.88	0.89	0.61	1.05
85		SC-12G-80	2890	0.86	0.88	0.57	1.09
86	Tang et al. [30]	fh-f-2	1589.63	0.67	0.69	0.47	0.81
87		fh-f-4	1317.76	0.68	0.70	0.46	0.85
88		fh-f-8	908.05	0.82	0.84	0.53	1.07
89		fl-f-2	1127.35	0.78	0.79	0.56	0.92
90		fl-f-4	824.88	0.86	0.87	0.60	1.05
91		fl-f-8	616.12	0.96	0.98	0.66	1.21
	Mean			0.92	0.94	0.64	1.04
	SD			0.125	0.128	0.089	0.136
	COV (%)			13.66	13.74	13.87	13.08
	MAPE			10.798	10.122	35.618	10.334

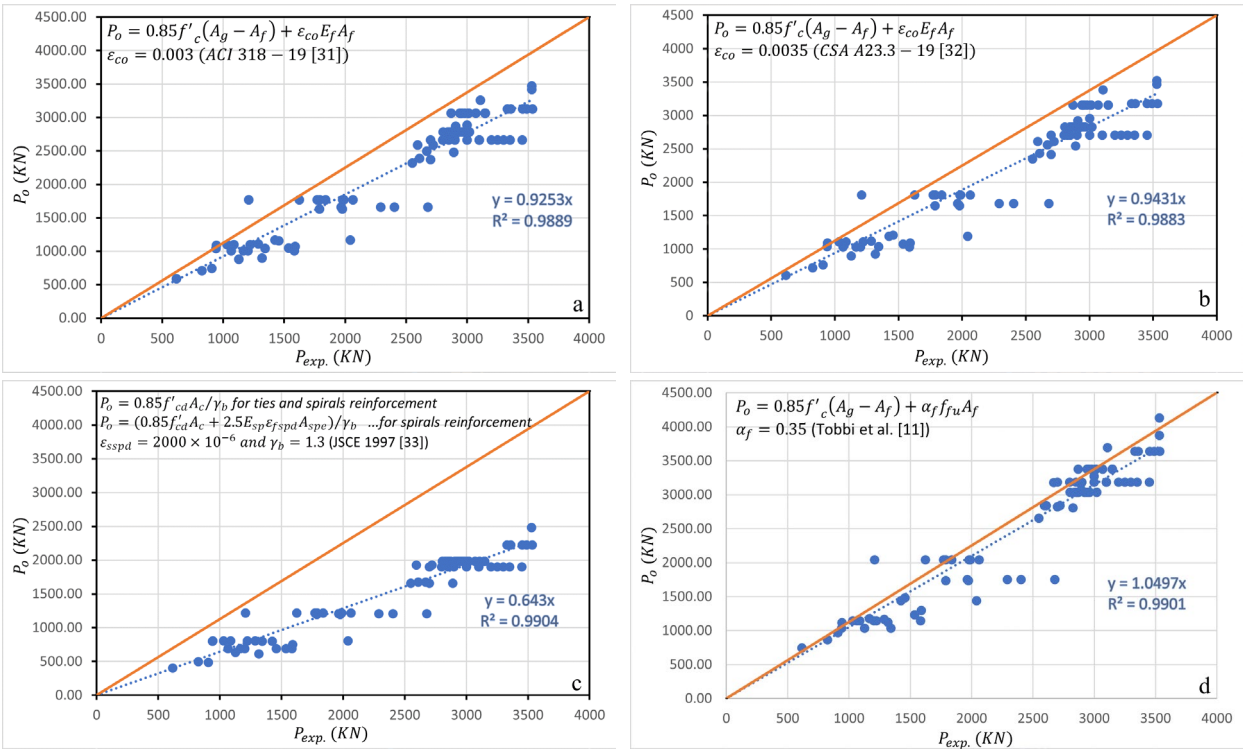

Figure 1. Experimental versus predicted axial load carrying capacity of FRP bar reinforced concrete columns obtained using: a) Eq. (5) (ε_{co} = 0.003); b) Eq. (5) (ε_{co} = 0.0035); c) Eq. (2.1 or 2.2) (γ_b =1.3); and d) Eq. (3) (α_f = 0.35).

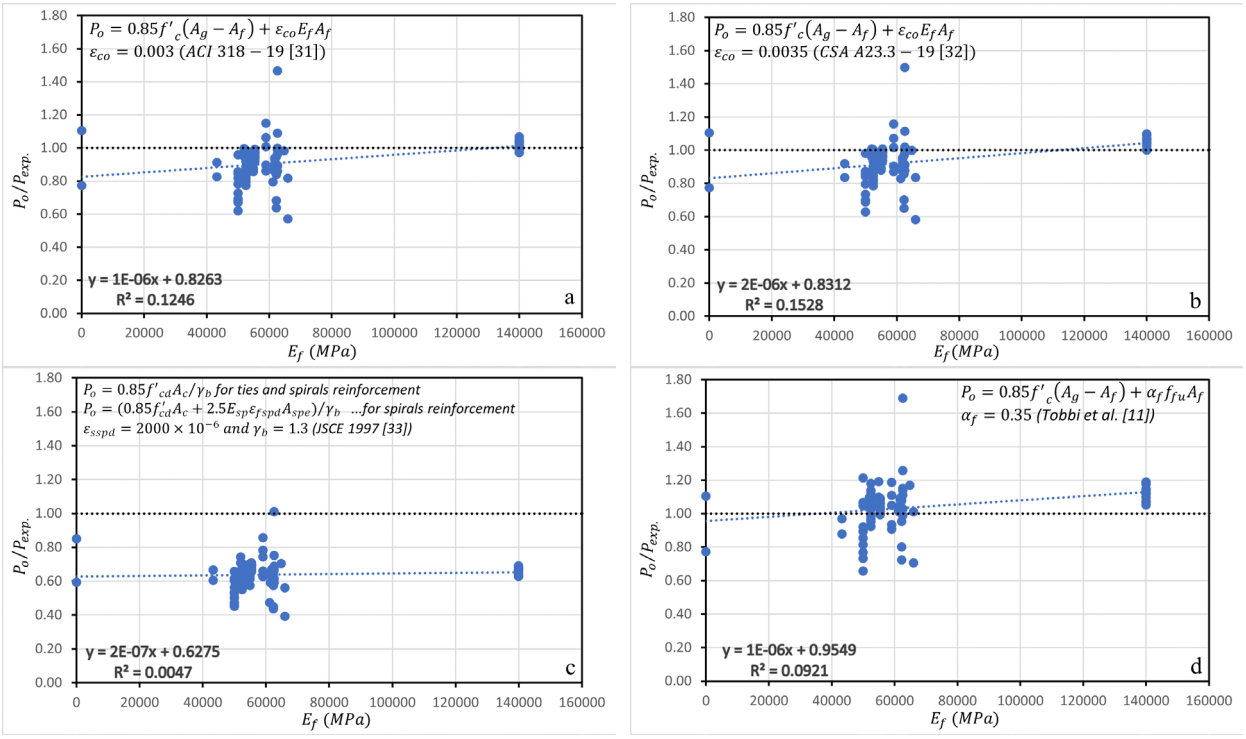

Figure 2. The relationship between $P_o / P_{exp.}$ of the FRP-bar reinforced concrete column and the modulus of elasticity of the reinforcement E_f. The following equations were used to calculate P_o: a) Eq. (5) (ε_{co} =0.003), b) Eq. (5), c) Eq. (2.1 or 2.2) (γ_b =1.3), and d) Eq. (3) (α_f = 0.35).

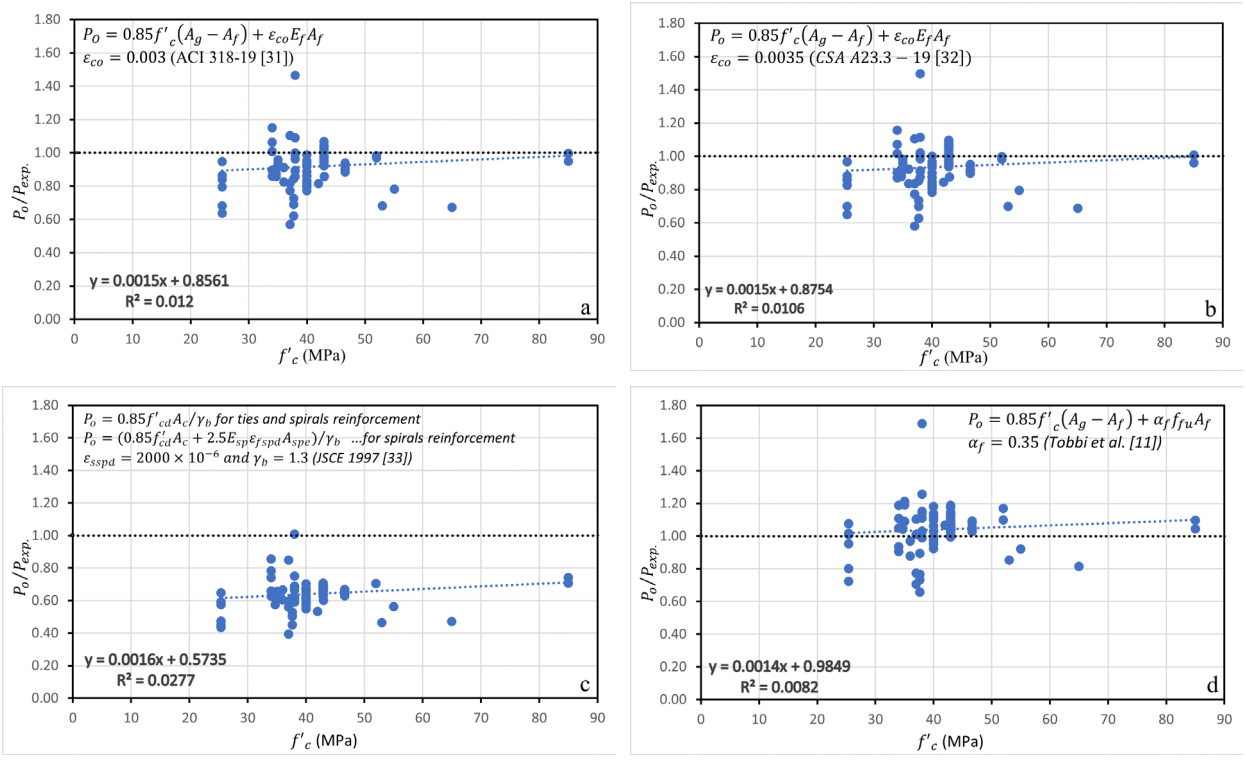

Figure 3. The relationship between $P_o / P_{exp.}$ of the FRP bar reinforced concrete column and the compressive strength of the concrete $f'c$. Note: P_o were calculated using: a) Eq. (5) (ε_{co} =0.003); b) Eq. (5) (ε_{co} =0.0035); c) Eq. (2.1 or 2.2) (γ_b =1.3); and d) Eq. (3) (α_f = 0.35).

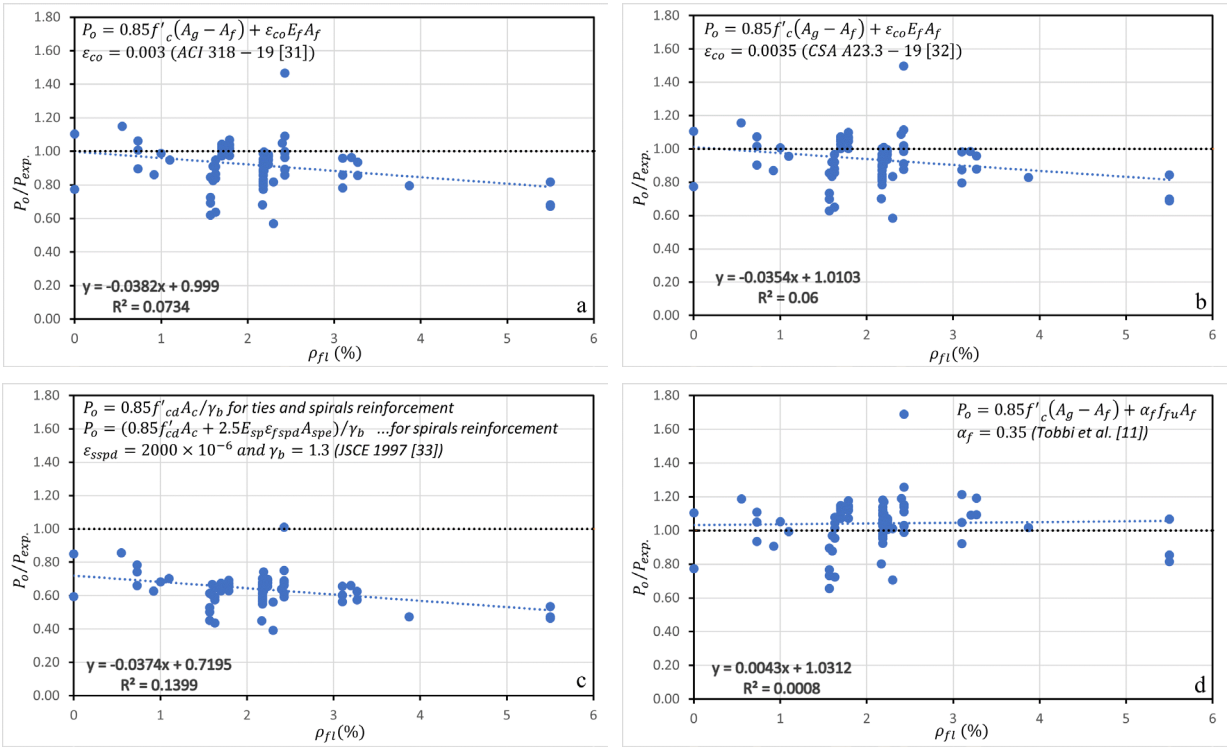

Figure 4. The relationship between $P_o / P_{exp.}$ of the FRP bar reinforced concrete column and the longitudinal reinforcement ratio ρ_{fl}. Note: P_o were found by using: a) Eq. (5) (ε_{co}=0.003), b) Eq. (5) (ε_{co}=0.0035), c) Eq. (2.1 or 2.2) (γ_b=1.3), and d) Eq. (3) (α_f = 0.35).

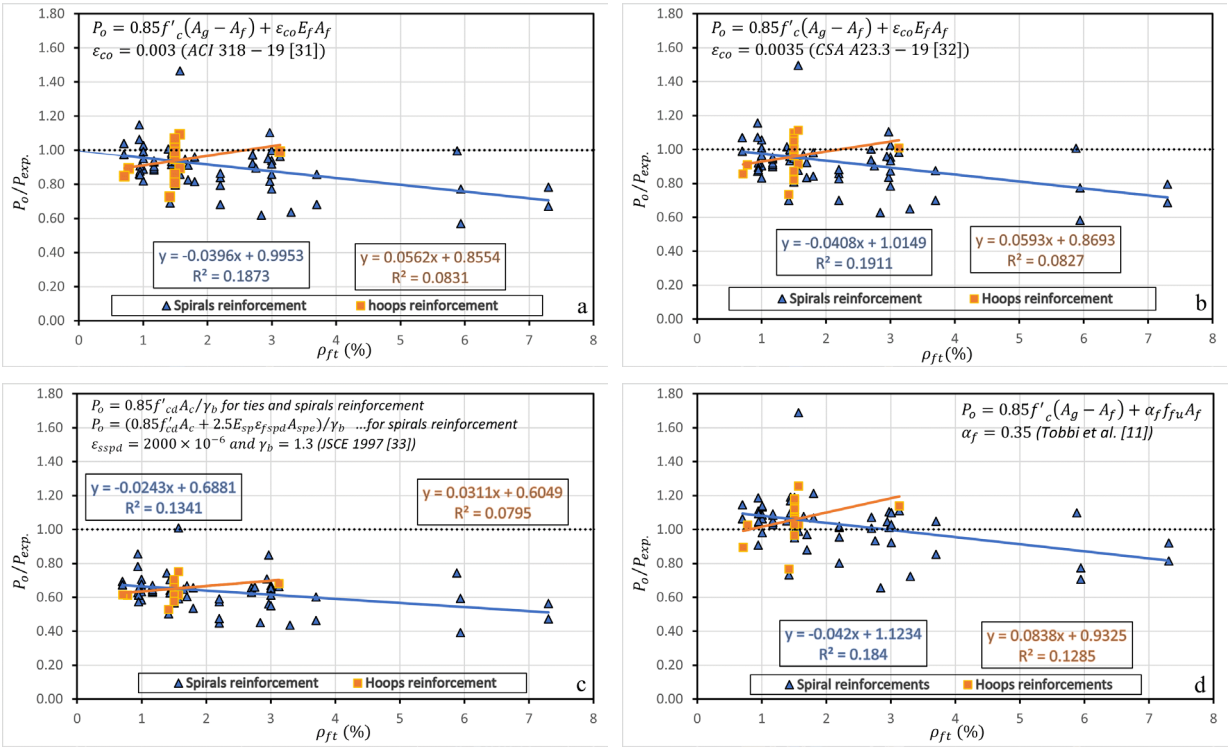

Figure 5. The relationship between $P_o / P_{exp.}$ and the transverse reinforcement ratio ρ_{ft} of the FRP bar reinforced concrete column. Note: P_o was calculated by using the equations: a) Eq. (5) (ε_{co}=0.003), b) Eq. (5) (ε_{co}=0.0035), c) Eq. (2.1 or 2.2) (γ_b=1.3), and d) Eq. (3) (α_f = 0.35).

3. Results and Discussion

3.1. Maximum axial load carrying capacity of reinforced concrete columns

This statistical study looks at theoretical equations to find the maximum axial load-carrying capacity of FRP bar-reinforced concrete columns under pure compression stresses. The previously proposed equations for the maximum axial load-carrying capacity of FRP bar-reinforced concrete columns can be used in future compound structure design codes. This research doesn't address the effect of combined axial and flexural loads on the behavior of FRP bar-reinforced concrete columns. Previous research studies used several equations to predict the maximum axial load-carrying capacity of FRP bar-reinforced concrete columns. It is critical to remember that the concrete's contribution to the analytically computed axial load-carrying capacity of FRP-bar reinforced concrete columns, remains similar in all of the proposed equations. In simpler terms, the differences in analytically derived P_o values for FRP bar-reinforced concrete columns are primarily due to the different concepts adopted in different equations for calculating the longitudinal bar contribution $\left(P_{bar,FRP}\right)$. As was mentioned above, the FRP bar's compressive strength is considerably lower than its tensile strength and the behavior of the FRP bar under compressive loads differs significantly. Therefore, ACI 440.1R-06 [34] suggests that FRP bars shouldn't be used to reinforce concrete columns longitudinally, and ACI 440.1R-15 [16] makes no recommendations about this. The CAN/CSA S806-12 [15] and JSCE 1997 [33] allow FRP bars to be used to reinforce concrete columns in a main direction. However, CAN/CSA S806-12 and JSCE 1997 [15, 33] say that the contribution of the FRP longitudinal bars should be ignored when estimating the maximum axial load-carrying capacity of FRP bar-reinforced concrete columns. Using the recommendations in CAN/CSA S806-12 and JSCE 1997 [15, 33], Eq. (1) and Eq. (2) can be used to predict the maximum axial load-carrying capacity of FRP bar-reinforced concrete columns.

$$P_o = 0.85 f_c' \left(A_g - A_f \right); \tag{1}$$

$$P_o = 0.85 f_c' A_c / \gamma_b ; \tag{2.1}$$

$$P_o = \left(0.85 f_c' A_e + 2.5 E_{sp} \varepsilon_{fspd} A_{spe} \right) \Big/ \gamma_b , \tag{2.2}$$

where A_f is the total cross-sectional area of FRP longitudinal bars, A_c is the cross-sectional area of concrete (mm^2), A_e is the cross-sectional area of concrete surrounded by spiral reinforcement, A_{spe} is the equivalent cross-sectional area of spiral reinforcement $\left(= \Pi d_{sp} A_{sp} / s\right)$, d_{sp} is the diameter of the concrete section surrounded by spiral reinforcement, A_{sp} is the cross-sectional area of spiral reinforcement, E_{sp} is the young's modulus of spiral reinforcement $\left(E_{fu}\right)$, ε_{fspd} is the design value for the strain of spiral reinforcement in the ultimate limit state, which is usually taken to be 2000×10^{-6}, γ_b is the member factor, which is generally taken to be 1.3, s is the pitch of spiral reinforcement. Note that JSCE 1997 [33] stated that when the members are subjected to axial compression force, the upper limit of axial compression capacity P_o will be calculated using Eq. (2.1) while hoops are used and either Eq. (2.1) or Eq. (2.2) whatever provides the biggest result, when spiral reinforcement is used. But a lot of research has shown that ignoring the contribution of FRP longitudinal bars in compression, as in Eq. (1–2.2), could cause a big difference between the analytically calculated axial load-carrying capacity of FRP bar reinforced concrete columns and the experimentally obtained value [12, 35, 36]. Consequently, two approaches were considered to compute the contribution of FRP longitudinal bars in the maximum axial load-carrying capacity of FRP bar-reinforced concrete columns. In the first approach, the axial load sustained by FRP longitudinal bars is calculated using the tensile strength of the FRP bars, $\alpha_f f_{fu} A_f$ (Equation (3)). In the second approach, the axial load sustained by FRP longitudinal bars is calculated using the axial strain in the FRP bars and the stiffness of the FRP bars, $\varepsilon_f E_f A_f$ (Eq. (4)).

$$P_o = 0.85 f_c' \left(A_g - A_f \right) + \alpha_f f_{fu} A_f ; \tag{3}$$

$$P_o = 0.85 f_c' \left(A_g - A_f \right) + \varepsilon_f E_f A_f . \tag{4}$$

In Eq. (3), the α_f is a reduction factor that represents the ratio between the strength of the FRP bar under compression and the strength of the FRP bar under tension. Different values for α_f were recommended in the previous studies. Alsayed et al. [10] suggested taking α_f equal to 0.6. Later, Tobbi et al. [11] recommended taking α_f equal to 0.35 based on experimental observations reported in Kobayashi and Fujisaki [8]. Moreover, α_f was recommended to be taken equal to 0.35 in Afifi et al. [18] for GFRP bar-reinforced circular concrete columns. Nevertheless, for CFRP bar-reinforced circular concrete columns, Afifi et al. [12] recommended taking α_f equal to 0.25. In Eq. (4), different values were also suggested for the axial strain in the FRP longitudinal bars, α_f, at the maximum axial load-carrying capacity of the concrete columns. Mohamed et al. [19] suggested taking ε_f equal to 0.002, explaining that this value $\left(\varepsilon_f = 0.002\right)$ represents the axial strain in the FRP longitudinal bars at the initiation of the micro-cracks in the plastic stage of the concrete. Nevertheless, Hadi et al. [36] recommended taking ε_f equal to 0.003, which represents the ultimate strain of the concrete, ε_{cu}. It is obvious that different research studies proposed different equations based on a limited number of experimental data. Therefore, there is no consensus in the previous research studies on a unified equation for predicting the maximum axial load-carrying capacity of FRP bar-reinforced concrete columns, which may also be attributed to the variances in the response of the FRP bars under axial compression. In this study, the axial load sustained by FRP longitudinal bars, $P_{bar,FRP}$, was predicted based on the stiffness (modulus of elasticity) of the FRP bars because the modulus of elasticity of FRP bars in compression is approximately similar to the modulus of elasticity of FRP bars in tension [7, 9]. Therefore, simply changing the value of the reduction factor α_f in Eq. (3) might not provide reasonable predictions for the maximum axial load-carrying capacity of FRP bar-reinforced concrete columns. The axial strain in the FRP longitudinal bars ε_f at the maximum axial load-carrying capacity of the concrete columns was considered to be equal to the concrete axial strain at peak stress ε_{co}. The concept adopted in this study is consistent with the assumption which states that the axial strain in the concrete and the axial strain in longitudinal FRP reinforcing bars are equal at any concentric axial load. Consequently, the maximum axial load-carrying capacity of FRP bar-reinforced concrete columns can be predicted using Eq. (5):

$$P_o = 0.85 f_c' \left(A_g - A_f \right) + \varepsilon_{co} E_f A_f . \quad (5)$$

3.2. Evaluation of the proposed and codes equations

3.2.1. Overall performance

In this study, the three code equations were assessed with a proposed equation from a previous study through the analysis of a large set of available experimental data (Table 1). This study examined the equation proposed by Tobbi et al. [8]. Hadi et al. [36] recommended assuming ε_f equal to ε_{cu}. The equation proposed by Hadi et al. [36] was also assessed. First, by taking ε_{cu} equal to 0.003 as defined in the ACI 318-19 [31] standard. Then, by taking ε_{cu} equal to 0.0035 as defined in the CSA A23.3-19 standard [32]. Table 3 presents the ratios between the analytically predicted and the experimentally obtained axial load carrying capacity $\left(P_o / P_{\text{exp.}}\right)$ for the experimentally tested specimens in Table 1. The analytically predicted axial load carrying capacity, P_o, was calculated by either using Eq. (3) by taking α_f equal to 0.35, as recommended by Tobbi et al. [11], or using Eq. (5), in which the value of ε_{co} was taken equal to ε_{cu} (0.003 or 0.0035, as defined in the ACI 318-19 [31] and CSA A23.3-19 [32], or using Eq. (2.1 and 2.2) from the JSCE 1997 [33], which depends mostly on the type of transverse reinforcement (hoops or spirals). The most optimal line for each equation is also shown alongside the experimental and theoretical axial load. The same number shows perfect performance. The equation with fewer scatters and better performance is one where the most optimal line and the plotted data are closer to the perfect line. Four

relationships $\left(f_c', \rho_{fl}, E_f, \text{ and } \rho_{ft}\right)$ are displayed to illustrate the ratio between the experimental axial load and the theoretical axial load using the selected equations for each tested column. In Table 3, four different mathematical measurements (Mean value (μ), Standard Deviation (SD), Coefficient of Variation (COV), and the Mean Absolute Percent Error (MAPE)) were used to evaluate the accuracy, consistency, and safety of the equations available according to three codes (ACI 318-19 [31], CSA A23.3-19 [32], and JSCE 1997 [33]) and according to only one proposed in one previous study (Tobbi et al. [11]). Among the unique values, the Mean value (μ) is the midpoint between the wide range of P_o. More precise results can be expected when the mean is closer to unity. The dispersion (variation) in P_o values was measured using the SD. For FRP bar-reinforced concrete specimens, a high SD indicates that the predicted axial load-carrying capacities fall within a wider range of values (less precisely) and a lower value SD indicates the opposite. The COV was then used to evaluate the dispersion of P_o values relative to the mean value as a percentage. As the COV decreases, performance becomes more stable and less variable from the mean. The MAPE is used to compare the accuracy of different equations used to determine the maximum axial load-carrying capacities of FRP-bar reinforced concrete columns. If the MAPE is small, then the equation should yield precise results. The most optimal line's slope indicates how consistently the performance meets or exceeds predictions for the chosen parameter. Table 3 shows a comparison of the experimental axial load-carrying capacity of FRP-bar-reinforced concrete columns to the theoretical value. It was noticed that Eq. (5), in which the contribution of the FRP bars is calculated based on their stiffness, is a more precise and safe way to predict P_o than Eq. (3), in which the contribution of the FRP bars is calculated based on their tensile strength. Eq. (5) is a safer and more reliable way to predict P_o than (2.1, 2.2), which uses transverse reinforcement. Possible explanations for this include the fact that despite significant differences between their tensile and compressive strengths, FRP bars have a modulus of elasticity that is nearly identical in tension and compression. Table 3 presents the SD and COV, which are 0.136 and 13.08, respectively, when P_o is calculated using Eq. (5), the equation proposed by Tobbi et al. [11]. This permits more consistent results. However, the lowest MAPE of 10.798 in predicting P_o was achieved by taking the concrete axial strain at peak stress $\varepsilon_{co} = 0.003$ in the computation of $P_{bar,FRP}$. By taking ε_{co} equal to 0.0035 when computing $P_{bar,FRP}$, predictions for $P_o/P_{\text{exp.}}$ with = 0.94, which is very close to unity and rather secure, but with high SD and COV of 0.128 and 13.74, respectively, were obtained (Fig. 1). As can be seen in Fig. 1, the SD and COV are 0.089 and 13.87, respectively, when using the Eq. (2.1, 2.2) that is available in JSCE is used to calculate $P_{bar,FRP}$, resulting in higher discrepant values of P_o. Thus, Eq. (5) which is available in CSA provides more realistic predictions than do those of other codes (ACI, JSCE). The axial load-carrying capacity of FRP bar-reinforced concrete columns was taken from previous studies and compared to the axial load-carrying capacity calculated using ACI 318-19 [31] and CSA A23.3-19 [32], respectively in Fig. 1. The JSCE's 1997 [33] equation and Tobbi et al.'s equation [11], were assessed. The slope of the trend line is 0.92 for the ACI, 0.94 for the CSA, 0.64 for the JSCE, and 1.04 for Tobbi. In addition, the axial load was calculated by using CSA and Tobbi equations, and that is more in line with the axial load measured experimentally. ACI, CSA, JSCE, and Tobbi each found a COV for axial load experimental versus a theoretical axial load of 13.66, 13.74, 13.87, and 13.08, respectively. The ACI and JSCE are less precise than the CSA. Finally, when comparing the Tobbi equation to the others that were considered, it was found to be the most precise in predicting the axial load-carrying capacity. Lastly, the performance tests on concrete compression design practices (Table 3) showed that the proposed equation by Tobbi et al. [11] with suitable safety factors had better optimization, followed by the CSA A23.3-19 [32] guidelines, the ACI 318-19 [31] code, and the JSCE 1997 guidelines [33]. The statistical tests yielded consistent results for the SD, COV, MAPE, and mean. The Tobbi et al. [11] design equation and the CSA A23.3-19 [32] guidelines did better than the ACI 318-19 [31] code, which had some extreme values because they had fewer conservative values. The JSCE 1997 [33] was not safe and had more conservative points than the other design methods because 97 % of their predictions were dangerous or extremely dangerous. Tobbi et al. [11], CSA A23.3-19 [32], and ACI 318-19 [31] showed better assessment because the $P_o/P_{\text{exp.}}$ was less conservative by 9, 19, and 23 %, respectively.

3.2.2. Young's modulus

For solids only, the stress (tension or compression) ratio to strain is known as Young's modulus or the main modulus of elasticity. This linear relationship between stress and strain expresses the extent of

flexibility of the material and explains how the material behaves under the influence of forces. This factor has a major effect on the axial load-carrying capacity of FRP-RC columns. The $P_o/P_{\text{exp.}}$ vs the E and the most optimal line trendlines from the database are shown in Fig. 2. As Young's modulus increases, so does the $P_o/P_{\text{exp.}}$ The most optimal lines for the ACI, CSA, JSCE, and Tobbi have an inclination of 1E-6, 2E-6, 2E-7, and 1E-6, respectively. Therefore, CSA provides greater consistency in terms of E value in terms of safety compared to ACI, JSCE, and Tobbi. The CSA equation can be inferred to be more reliable for FRP types than any of the chosen equations.

3.2.3. Concrete strength

One measure of a material's or structure's durability is its compressive strength, or how well it carries up under compression stresses. The axial load-carrying capacity of FRP-RC columns is significantly impacted by this factor. The $P_o/P_{\text{exp.}}$ vs f_c' and the most optimal line trendline using the proposed and selected equations are shown in Fig. 3. The P_o calculated using Eq. (3) by taking α_f equal to 0.35 as recommended by Tobbi et al. [11], using Eq. (5) by taking ε_{co} equal to 0.003 as defined in the ACI 318-19 [31] and equal to 0.0035 as defined in the CSA A23.3-19 [32] or calculated using the Eq. (2.1, 2.2) as recommended in JSCE 1997 [33] are shown in Fig. 3. The axial load-carrying capacity for the majority of the FRP bar-reinforced NSC and HSC columns provided in Table 1 is well predicted using an assumption of α_f equal to 0.35 (Eq. (3)), as suggested by Tobbi et al. [11], as illustrated in Fig. 3a. The performance indicator $P_o/P_{\text{exp.}}$ tends to rise as f_c' gets higher. The slope of the line that provides the best match has an inclination of 1.5E-3 for the ACI, 1.5E-3 for the CSA, 1.6E-3 for the JSCE, and 1.4E-3 for the Tobbi. In terms of f_c' safety, the CSA is more reliable than the ACI and the JSCE. The Tobbi also exhibits the greatest degree of consistency with respect to f_c' of any of the chosen equations.

3.2.4. The longitudinal reinforcement ratios

The longitudinal reinforcement ratio, ρ_{fl}, is calculated by dividing the area of the longitudinal reinforcement by the cross-sectional area of the column. It is a significant factor affecting the axial load-carrying capacity of FRP-RC columns. The fluctuation in $P_o/P_{exp.}$ with longitudinal reinforcement ratio, according to the database, is shown in Fig. 4. As the reinforcement ratio rises, it can be seen that the $P_o/P_{exp.}$ has a decreasing trend. In addition, the slope of the most optimal line for the ACI, CSA, JSCE, and Tobbi is -38.2E-3, -35.4E-3, -37.4E-3, and +4.3E-3, respectively. Compared to CSA, JSCE, and Tobbi, ACI points are less crowded and closer to the perfect horizontal line. Consequently, ACI safety is more consistent concerning the ρ_{fl} value than CSA, JSCE, and Tobbi. It may be inferred that the ACI equation is more consistent for the FRP type than it is for the other equations considered.

3.2.5. Transverse reinforcement ratio

3.2.5.1. Spiral reinforcement ratio

The $P_o/P_{\text{exp.}}$ vs ρ_{ft} and the most optimal line trendline are shown in Fig. 5. The slope of the most optimal lines is -39.6E-3, -40.8E-3, -24.3E-3, and -4.2E-2 for the ACI, CSA, JSCE, and Tobbi, in that order. As ρ_{ft} increases, $P_o/P_{\text{exp.}}$ decreases. This suggests that the performance of spiral reinforcement improves when the distances are increased but within the applicable limits. In addition, the ACI is more consistent regarding ρ_{ft} safety than the Tobbi and JSCE. Finally, the CSA equation is more consistent concerning with respect to ρ_{ft} than any of the selected equations.

5.5.2. Hoops reinforcement ratio

The $P_o/P_{\text{exp.}}$ vs ρ_{ft} and the most optimal line trendline are shown in Fig. 5. For the ACI, CSA, JSCE, and Tobbi, the slope of the most optimal line is 56.2E-3, 59.3E-3, 31.1E-3, and 83.8E-2, respectively. Generally, there is a clear increase in $P_o/P_{\text{exp.}}$ with each increase in the ρ_{ft}. This indicates that hoop

reinforcement gives better performance when the spacings are smaller but within the applicable limits. In addition, the safety of the ACI is more consistent concerning the ρ_{ft} than that of the CSA and JSCE. Furthermore, the Tobbi outperforms the codes in terms of ρ_{ft} consistency. Finally, the behavior of the most optimal line trendlines for spiral reinforcement is clear that it is the opposite of the behavior of the perfect line for hoops reinforcement. Also, the ACI and the CSA provide better results than the JSCE in general, although Tobbi provides perfect results better than all other codes at least in the hoops reinforcement, and the results are close For the ACI and CSA in spirals reinforcement.

4. Conclusions

An extensive experimental database comprising 91 circular FRP-reinforced concrete columns was utilized to investigate the interrelation of geometry and details of circular FRP-reinforced concrete columns. The axial load-carrying capacity of the experimental database was determined using selected design codes and guidelines with one equation proposed in earlier research, the CSA design code exhibited superior precision compared to JSCE and ACI but less compared with Tobbi. The mean safety factors for JSCE, ACI, CSA, and Tobbi were found to be 0.64, 0.93, 0.94, and 1.04, respectively. JSCE showed less consistency and a significantly more conservative behavior compared to ACI, CSA, and Tobbi while ignoring the contribution of longitudinal bars and ultimate axial strain, which leads to an increase in implementation costs. Key distinctions between FRP-reinforced concrete columns and conventional steel-reinforced concrete columns were considered, such as varying FRP types (Young's modulus: 0–140 GPa), compressive failure due to concrete crushing without yielding FRP reinforcements, and increased deformation experienced by FRP-reinforced concrete columns. To validate the accuracy of the codes and the previously proposed equation, the experimental axial load-carrying capacity was compared with the predicted axial load-carrying capacity using equations for a large experimental database of reinforced concrete circular columns with FRP reinforcements. Tobbi's equation showed good agreement with experimental loads compared to other equations, which can be a good conclusion due to the remarkable complexity in the behavior of FRP bars and the big difference in the behavior of these bars in compression and tension. The analysis investigated the effects of concrete strength, FRP Young's modulus, longitudinal reinforcement ratio, and transverse reinforcement ratio on the results. These results showed the $P_o/P_{\exp.}$ of FRP-reinforced concrete columns increases with an increase in the value of the FRP Young's modulus, the longitudinal reinforcement ratio, and the concrete strength, respectively; and Tobbi's equation adequately accounted for the concrete strength and the hoops reinforcement effect. When the type is hoops, $P_o/P_{\exp.}$ increases as the ρ_{ft} increases, but when the type is spiral, $P_o/P_{\exp.}$ decreases as the ρ_{ft} increases. Finally, Tobbi's equation has the lowest COV compared with all code's equations and the best average nearing unity. However, MAPE for Tobbi is greater than CSA but less than JSCE and ACI, which require more experimental testing and more exact test measurements.

References

1. Sheikh, M.N., Légeron, F. Performance based seismic assessment of bridges designed according to canadian highway bridge design code. Canadian Journal of Civil Engineering. 2014. 41(9). Pp. 777–787. DOI: 10.1139/cjce-2013-0025
2. Zaman, A., Gutub, S.A., Wafa, M.A. A review on FRP composites applications and durability concerns in the construction sector. Journal of Reinforced Plastics and Composites. 2013. 32(24). Pp. 1966–1988. DOI: 10.1177/0731684413492868
3. Mukhopadhyay, T, Dey, T.K., Chowdhury, R., Chakrabarti, A., Adhikari, S. Optimum design of FRP bridge deck: an efficient RS-HDMR based approach. Structural and Multidisciplinary Optimization. 2015. 52(3). Pp. 459–77. DOI: 10.1007/s00158-015-1251-y
4. Li, X., Lu, J., Ding, D.D., Wang, W. Axial strength of FRP-confined rectangular RC columns with different cross-sectional aspect ratios. Magazine of Concrete Research. 2017. 69(19). Pp. 1011–1026. DOI: 10.1680/jmacr.17.00036
5. Karsh, P.K., Mukhopadhyay, T., Dey, S. Spatial vulnerability analysis for the first ply failure strength of composite laminates including effect of delamination. Composite Structures. 2018. 184. Pp. 554–567. DOI: 10.1016/j.compstruct.2017.09.078
6. American Concrete Institute (ACI) Committee 440. Report on Fiber-Reinforced Polymer (FRP) Reinforcement for Concrete Structures. ACI 440R-07. 2007. 100.
7. De Luca, A., Matta, F., Nanni, A. Behavior of full-scale glass fiber-reinforced polymer reinforced concrete columns under axial load. ACI Structural Journal. 2010. 107(5). Pp. 589–596.
8. Kobayashi, K., Fujisaki, T. 32 compressive behavior of FRP reinforcement in non-prestressed concrete members. Non-Metallic (FRP) Reinforcement for Concrete Structures: Proceedings of the Second International RILEM Symposium. First edition. Ghent E & FN Spon, an imprint of Chapman and Hall. 1995. 29. Pp. 267–274.
9. Deitz, D.H., Harik, I.E., Gesund, H. Physical properties of glass fiber reinforced polymer rebars in compression. Journal of Composites for Construction. 2003. 7 (4). Pp. 363–366. DOI: 10.1061/(ASCE)1090-0268(2003)7:4(363)
10. Alsayed, S.H., Al-Salloum, Y.A., Almusallam, T.H., Amjad, M.A. Concrete columns reinforced by glass fiber reinforced polymer rods. ACI Special Publication. 1999. 188. 103–112. DOI: 10.14359/5614

11. Tobbi, H., Farghaly, A.S., Benmokrane, B. Concrete columns reinforced longitudinally and transversally with glass fiber-reinforced polymer bars. ACI Structural Journal. 2012. 109(4). Pp. 551–558.
12. Afifi, M.Z., Mohamed, H.M., Benmokrane, B. Strength and axial behavior of circular concrete columns reinforced with CFRP bars and spirals. Journal of Composites for Construction. 2014. 18(2). 04013035. DOI: 10.1061/(ASCE)CC.1943-5614.0000430
13. Hadhood, A., Mohamed, H.M., Benmokrane, B. Experimental study of circular high-strength concrete columns reinforced with gfrp bars and spirals under concentric and eccentric loading. Journal of Composites for Construction. 2017. 21(2). 04016078. DOI: 10.1061/(ASCE)CC.1943-5614.0000734
14. Hadi, M.N., Hasan, H.A., Sheikh, M.N. Experimental investigation of circular high-strength concrete columns reinforced with glass fiber-reinforced polymer bars and helices under different loading conditions. Journal of Composites for Construction. 2017. 21(4). 04017005.
15. CAN/CSA S806-12. CSA (Canadian Standards Association). Design and construction of building structures with fibre-reinforced polymers (CAN/CSA S806-12). CAN/CSA S806-12. 2012. (Reaffirmed).
16. ACI440.1R-15. Guide for the design and construction of structural concrete reinforced with firber-reinforced polymer (FRP) bars. American Concrete Institute. 2015.
17. Pantelides, C.P., Gibbons, M.E., Reaveley, L.D. Axial load behavior of concrete columns confined with GFRP spirals. Journal of Composites for Construction. 2013. 17(3). Pp. 305–313.
18. Afifi, M.Z., Mohamed, H.M., Benmokrane, B. Axial capacity of circular concrete columns reinforced with GFRP bars and spirals. Journal of Composites for Construction. 2014. 18(1). 04013017. DOI: 10.1061/(ASCE)CC.1943-5614.0000438
19. Mohamed, H.M., Afifi, M.Z., Benmokrane, B. Performance evaluation of concrete columns reinforced longitudinally with FRP bars and confined with FRP hoops and spirals under axial load. Journal of Bridge Engineering. 2014. 19(7). 04014020. DOI: 10.1061/(ASCE)BE.1943-5592.0000590
20. Karim, H., Noel-Gough, B., Sheikh, M.N., Hadi, M.N. Strength and ductility behavior of circular concrete columns reinforced with GFRP bars and helices. In: FRPRCS-12/APFIS-2015 – Joint Conference of the 12th International Symposium on Fiber Reinforced Polymers for Reinforced Concrete Structures, FRPRCS 2015 and the 5th Asia-Pacific Conference on Fiber Reinforced Polymers in Structures, APFIS 2015. 2015.
21. Maranan, G.B., Manalo, A.C., Benmokrane, B., Karunasena, W., Mendis, P. Behavior of concentrically loaded geopolymer-concrete circular columns reinforced longitudinally and laterally with GFRP bars. Engineering Structures. 2016. 117. Pp. 422–436. DOI: 10.1016/j.engstruct.2016.03.036
22. Hadhood, A., Mohamed, H.M., Benmokrane, B. Failure envelope of circular concrete columns reinforced with glass fiber-reinforced polymer bars and spirals. ACI Structural Journal. 2017. 114(6). Pp. 1417–1428. DOI: 10.14359/51689498
23. Abdelazim, W., Mohamed, H.M., Benmokrane, B. Effect of slenderness ratio on the performance of concrete columns reinforced with GFRP bars and spirals. Proceedings, Annual Conference – Canadian Society for Civil Engineering. 2019.
24. Raza, A., Khan, Q.U.Z. Experimental and theoretical study of GFRP hoops and spirals in hybrid fiber reinforced concrete short columns. Materials and Structures. 2020. 53(6). 139. DOI: 10.1617/s11527-020-01575-9
25. El-Gamal, S., Al-Shareedah, O. Behavior of axially loaded low strength concrete columns reinforced with GFRP bars and spirals. Engineering Structures. 2020. 216. 110732. DOI: 10.1016/j.engstruct.2020.110732
26. Elchalakani, M., Dong, M., Karrech, A., Mohamed Ali, M.S., Huo, J.S. Circular concrete columns and beams reinforced with gfrp bars and spirals under axial, eccentric, and flexural loading. Journal of Composites for Construction. 2020. 24(3). 04020008. DOI: 10.1061/(ASCE)CC.1943-5614.0001008
27. Elhamaymy, A., Mohamed, H.M., Benmokrane, B. Durability assessment and behavior under axial load of circular GFRP-RC piles conditioned in severe simulated marine environment. Engineering Structures. 2021. 249. 113376. DOI: 10.1016/j.engstruct.2021.113376
28. Bakouregui, A.S., Mohamed, H.M., Yahia, A., Benmokrane, B. Axial load–moment interaction diagram of full-scale circular LWSCC columns reinforced with BFRP and GFRP bars and spirals: experimental and theoretical investigations. Engineering Structures. 2021. 242. 112538. DOI: 10.1016/j.engstruct.2021.112538
29. Gouda, M.G., Mohamed, H.M., Manalo, A.C., Benmokrane, B. Behavior of hollow glass fiber-reinforced polymer-reinforced concrete columns under axial load: experimental and theoretical investigation. ACI Structural Journal. 2022. 119(6). Pp. 289–302. DOI: 10.14359/51736117
30. Tang, Y., Sun, Z., Wei, Y., Zou, X. Compressive behavior and design method of BFRP bars constrained with a BFRP spiral with different spacings in concrete members. Engineering Structures. 2022. 268. 114757. DOI: 10.1016/j.engstruct.2022.114757
31. ACI (American Concrete Institute). Building Code Requirements for Structural Concrete (ACI 318-19) Commentary on Building Code Requirements for Structural Concrete (ACI 318R-19) IN-LB. 2019.
32. CSA (Canadian Standards Association). Design of concrete structures. CAN/CSA A23.3:19.
33. Japan Society of Civil Engineers (JSCE). Recommendation for Design and Construction of Concrete Structures Using Continuous Fiber Reinforcing Materials. Concrete Engineering Series 23, Research Committee on Continuous Fiber Reinforcing Materials. 1997; 23.
34. ACI (American Concrete Institute). Guide for the design and construction of structural concrete reinforced with FRP bars, ACI 440.1R-06 ACI (American Concrete Institute). Farmington Hills, MI. 2006.
35. Tobbi, H., Farghaly, A.S., Benmokrane, B. Behavior of concentrically loaded fiber-reinforced polymer reinforced concrete columns with varying reinforcement types and ratios. ACI Structural Journal. 2014. 111(2). Pp. 375–86. DOI: 10.14359/51686528
36. Hadi, M.N., Karim, H., Sheikh, M.N. Experimental investigations on circular concrete columns reinforced with GFRP bars and helices under different loading conditions. Journal of Composites for Construction. 2016. 20(4). 04016009. DOI: 10.1061/(ASCE)CC.1943-5614.0000670

Information about authors:

Mohamed Qassim Kadhim, *Master of Structural Engineering*
ORCID: https://orcid.org/0009-0007-0037-6453
E-mail: mohamedq1992@uomustansiriyah.edu.iq

Hassan Falah Hassan, *PhD*
ORCID: https://orcid.org/0000-0003-4610-0560
E-mail: hassanfalah@uomustansiriyah.edu.iq

Received 15.02.2023. Approved after reviewing 19.10.2023. Accepted 22.10.2023.